molecules

MDPI

Article

Molecular-Level Insights into CO_2 Dissolution Trapping in Deep Saline Aquifers: Diffusion Behavior in NaCl Brines

Tiankuo Zhou [1] and Dexiang Li [2,*]

[1] SDU-ANU Joint Science College, Shandong University, Weihai 264209, China; 202300700155@mail.sdu.edu.cn
[2] School of Nuclear Science, Energy and Power Engineering, Shandong University, Jinan 250061, China
* Correspondence: de-xiang.li@sdu.edu.cn; Tel.: +86-13730981950

Abstract

Carbon capture, utilization, and storage (CCUS) is critical for carbon neutrality, and deep saline aquifers are promising reservoirs for CO_2 sequestration. CO_2 diffusion in brine directly affects dissolution trapping efficiency and is strongly influenced by salt ions. Molecular dynamics simulations were employed to investigate CO_2 diffusion in NaCl brines under varying concentrations (0.1–5.0 mol/L), temperatures (298–353 K), and pressures (3–40 MPa). Diffusion coefficients were derived from mean square displacement, and radial distribution functions combined with hydrogen bond analysis were used to elucidate microscopic mechanisms. Results show that as NaCl concentration increases from 0.1 to 5.0 mol/L, the diffusion coefficient decreases by ~50%, reflecting the kinetic consequence of the salting-out effect. Raising temperature from 298 to 353 K enhances diffusion by ~149%, following Arrhenius behavior, while pressure shows negligible influence below 30 MPa but causes a 15% drop at 40 MPa. RDF analysis reveals that higher salinity densifies the CO_2 hydration shell without changing its coordination number, and ions do not accumulate near CO_2. Hydrogen bond analysis indicates that slower diffusion arises primarily from increased viscosity and steric hindrance from hydrated ions rather than disruption of hydrogen bonds. These molecular-level insights can guide site selection and injection strategy optimization for CO_2 geological storage in saline aquifers.

Keywords: CO_2 geological storage; saline aquifer; molecular dynamics simulation; diffusion coefficient; salt concentration

1. Introduction

Global climate change continues to intensify, and cutting greenhouse gas emissions has become urgent. Consequently, carbon capture, utilization, and storage (CCUS) has emerged as a critical strategy for achieving carbon neutrality [1,2]. The Global CCS Institute reported that the global CO_2 capture capacity was 416 Mtpa in 2024, more than double the 2017 level. However, the capacity currently in operation remains far below the gigaton-scale level needed by 2050 under the IEA's Net Zero Emissions Scenario [3,4]. The IPCC Special Report on CCS noted that deep saline aquifers have the largest storage capacity among geological storage options, estimated at 1000–10,000 Gt CO_2 globally, owing to their wide geographical distribution and substantial storage potential [5,6]. When CO_2 is injected into saline aquifers, its diffusion behavior directly governs the efficiency of dissolution trapping and affects the long-term safety of CO_2 storage [7]. Therefore, a comprehensive understanding of CO_2 diffusion in brine under realistic reservoir conditions is essential

Check for updates

Academic Editor: Jose C. Corchado

Received: 21 May 2026
Revised: 6 June 2026
Accepted: 8 June 2026
Published: 11 June 2026

Copyright: © 2026 by the authors. Licensee MDPI, Basel, Switzerland. This article is an open access article distributed under the terms and conditions of the Creative Commons Attribution (CC BY) license.

for selecting appropriate storage sites, assessing risks, and designing injection strategies in CCUS projects.

Among CO_2 emission reduction technologies, CCUS has attracted substantial research attention. Before CO_2 is injected into saline aquifers, the gas captured from industrial sources typically requires compression and purification—processes that incur substantial costs [8]. Izadpanahi et al. recently reviewed all four CO_2 trapping mechanisms in saline aquifers—structural, residual, dissolution, and mineralization—and concluded that dissolution trapping is the key bridging mechanism that dominates during injection and the early post-injection phase [9]. However, natural saline aquifers typically contain ions such as Na^+ and Cl^-, and these ions can significantly alter the microscopic structure and physical properties of water, thereby affecting CO_2 transport and diffusion [10]. Systematically characterizing CO_2 diffusion across a range of salinity conditions is essential for assessing CO_2 migration behavior and long-term trapping efficiency in realistic geological formations.

Dissolution trapping in saline aquifers involves several physical and chemical steps: CO_2 dissolves at the gas-brine boundary, molecules diffuse through the boundary layer, and density differences in the brine cause convective mixing. Among these, molecular diffusion is the rate-limiting step that controls the long-term dissolution rate after the early convection dies down [11]. In recent years, molecular dynamics (MD) simulation has become a powerful tool for understanding transport mechanisms at the atomic scale. Zhang et al. reviewed microscopic simulation methods for CO_2–water–rock systems [12]. They noted that MD can capture molecular interaction details beyond the reach of continuum models, including ion-specific hydration, hydrogen bond dynamics, and local structural ordering around dissolved gases. Coelho et al. studied the Soret effect of CO_2 in NaCl brines using non-equilibrium MD [13]. They found that as temperature rises, CO_2 switches from thermophobic to thermophilic behavior. This change is mainly attributed to alterations in the water hydrogen bond network, rather than direct ion–CO_2 interactions. These findings demonstrate that molecular-level work is essential for building reliable predictive models of CO_2 transport in saline aquifers.

The composition of saline aquifers and the corresponding CO_2 diffusion behavior significantly influence storage performance. Saline aquifers are predominantly composed of water with dissolved ions such as Na^+ and Cl^-. CO_2 diffusion in this water is driven by concentration gradients, but it is also modulated by temperature and pressure [14]. Zhang et al. used field-scale simulations and showed that brine salinity is a key factor controlling the relative contributions of dissolution trapping and residual trapping. Higher salinity reduces CO_2 solubility because of the salting-out effect [15]. Previous work by Carroll et al. demonstrated that salt ions generally reduce CO_2 solubility in water—this is the well-documented salting-out effect [16]. Chen et al. used MD to investigate ion hydration and hydrogen bond structure in NaCl solutions under CO_2 storage conditions. They found that dissolved CO_2 disrupts the hydrogen bond network and destabilizes ionic hydration shells [17]. These findings indicate that the salting-out effect is not solely a solubility-related phenomenon—it also has a kinetic dimension that directly affects CO_2 transport. However, a systematic molecular-level investigation quantifying the combined effects of salt concentration, temperature, and pressure on CO_2 diffusion remains absent.

Deep saline aquifers offer the largest CO_2 storage capacity among geological formations, and formation brine is often used directly as the injection fluid [11]. Omrani et al. showed that when salinity increases, the CO_2 diffusion coefficient decreases, which can retard CO_2 movement in the reservoir and inhibit dissolution trapping efficiency [18]. Song et al. provided a comprehensive molecular simulation framework for understanding geological carbon storage [19]. This framework covers solubility trapping, interfacial phenomena, and adsorption mechanisms using both MD and Monte Carlo methods. Li et al.

recently showed that external physical fields can change CO_2 dissolution at the molecular scale; for example, electric fields can boost the dissolution rate by up to 42% by reorienting water dipoles at the interface [20]. These findings suggest that a deeper understanding of molecular-scale transport could lead to new engineering strategies for improved CO_2 storage. Deep saline aquifers are cost-effective and secure options for CO_2 storage, and the interactions between CO_2 and formation brine are fundamental to securing long-term storage [21]. Temperature, pressure, and water chemistry all influence CO_2 diffusion. Changes in salinity affect both ionic strength and water activity, thereby altering the CO_2 diffusion coefficient. Because salinity varies spatially in natural aquifers and cannot be engineered for storage purposes, systematic studies on CO_2 diffusion behavior across salinity gradients represent a fundamental research need.

To obtain reliable diffusion data, a CO_2–brine model that matches real saline aquifer conditions must be constructed, and MD simulations must be run at realistic temperatures and pressures. We performed MD simulations spanning NaCl concentrations of 0.1–5.0 mol/L, temperatures of 298–353 K, and pressures of 3–40 MPa. Diffusion coefficients were derived from MSD, and RDF combined with hydrogen bond analyses was used to resolve the underlying molecular mechanisms. The results quantify the competing effects of salinity, temperature, and pressure on CO_2 diffusivity and identify viscosity enhancement—rather than hydrogen bond disruption—as the primary mechanism by which salt ions retard CO_2 transport.

2. Results and Discussion

2.1. CO_2 Diffusion Coefficients Under Varying Salinity, Temperature, and Pressure

The CO_2 diffusion coefficients in brine under different salinity, temperature, and pressure conditions were obtained from the MD simulations. By analyzing the MSD, we compared and quantified the influence of these three factors on CO_2 diffusion. Figure 1 presents the Arrhenius plot confirming the thermally activated nature of CO_2 diffusion, while Figure 2 provides a comprehensive overview of the diffusion coefficient as a function of all three variables.

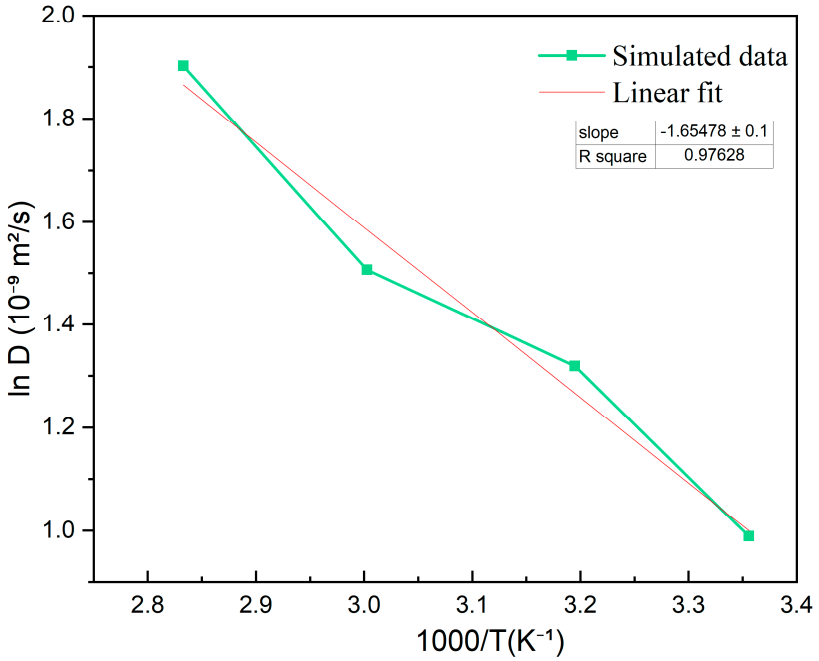


Figure 1. Arrhenius plot of the CO_2 diffusion coefficient in brine at 3.5 mol/L NaCl and 10 MPa. The linear fit yields an activation energy of 13.8 kJ/mol.

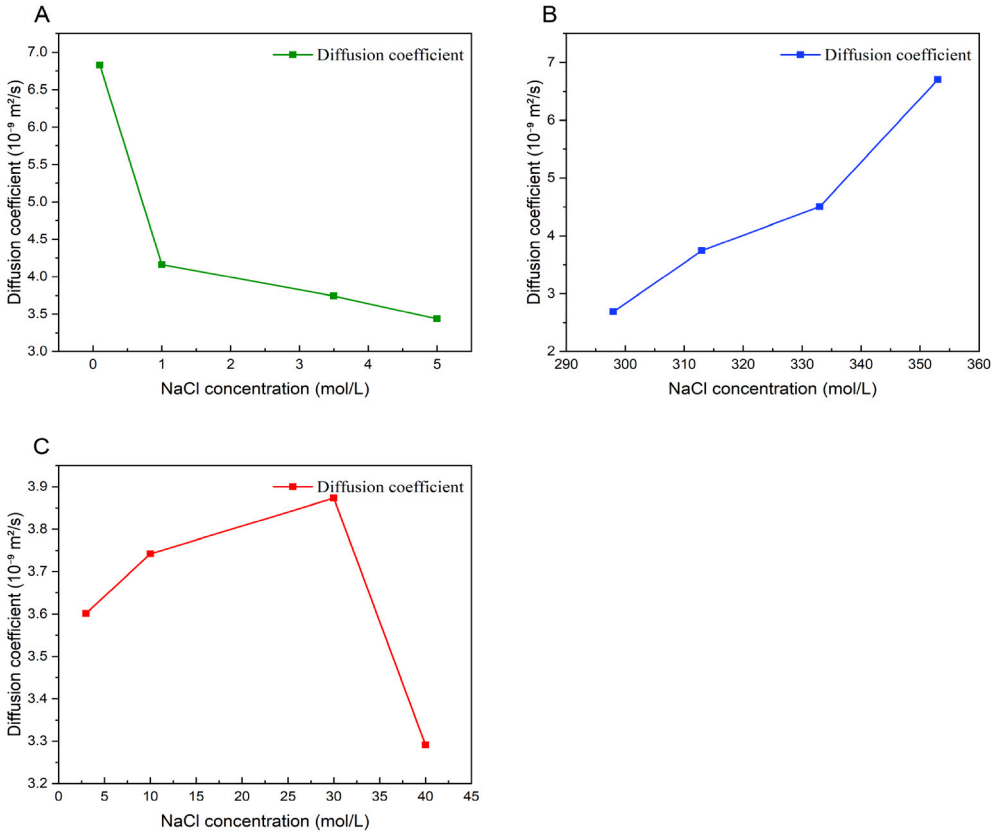


Figure 2. Diffusion coefficient of CO_2 in brine as a function of (**A**) NaCl concentration, (**B**) temperature, and (**C**) pressure.

2.1.1. Influence of Salinity

Figure 2A plots the CO_2 diffusion coefficient against NaCl concentration at 313 K and 10 MPa. As salinity increases from 0.1 to 5.0 mol/L, coefficient D decreases by approximately 49.6% (from 6.83×10^{-9} to 3.44×10^{-9} m^2/s), consistent with the well-documented salting-out effect [16]. The decline is more pronounced at low concentrations (0.1 → 1.0 mol/L accounts for ~39% of the total decrease) and attenuates at higher concentrations (3.5 → 5.0 mol/L accounts for only ~8%). This non-linear behavior arises because ionic hydration shells gradually saturate. At low salinity, added ions hydrate strongly and sequester free water molecules, which rapidly increases the solution viscosity and retards CO_2 diffusion. As concentration increases, the hydration shells are nearly saturated, and therefore adding more ions has a diminished effect on the solution structure. The RDF analysis in Section 2.2.1 supports this: the first hydration shell of CO_2 becomes denser (higher peak, narrower FWHM) with salinity, but it does not incorporate more water molecules. The hydrogen bond analysis in Section 2.3 provides further support: the CO_2–water hydrogen bond count decreases by only ~5% over the same salinity range. The dominant mechanism is therefore increased solution viscosity rather than direct ion blocking.

2.1.2. Influence of Temperature

Figure 1 shows that ln D and 1000/T have a clear linear relationship at 3.5 mol/L NaCl and 10 MPa, indicating that CO_2 diffusion follows Arrhenius behavior. The activation energy obtained from the fit is 13.8 kJ/mol, which is well within the range of 13.5–16.2 kJ/mol that Omrani et al. [18] reported under similar salinity, supporting the consistency of the present results. Figure 2B shows the corresponding temperature trend: when the temperature increases from 298 to 353 K, coefficient D increases from 2.69×10^{-9}

to 6.70×10^{-9} m^2/s—an increase of approximately 149%, consistent with the enhanced molecular mobility at elevated temperatures [18].

At the molecular level, E_a is the energy barrier CO_2 molecules must overcome to escape from the surrounding water and ions and make a diffusive jump. The activation energy obtained is higher than the typical value for CO_2 in pure water, which indicates that salt ions impede diffusion. However, temperature enhances diffusion to a greater extent than salinity suppresses it. As described in Section 2.2, higher temperature disrupts the ordered hydration shell (the RDF peak decreases in height and broadens), reduces local viscosity and lowers the barrier for CO_2 to escape from its hydration cage. Even at the high salinity of 3.5 mol/L NaCl, the CO_2 diffusion coefficient at 353 K (6.70×10^{-9} m^2/s) remains substantially higher than the value of 3.08×10^{-9} m^2/s reported by Perera et al. in pure water at 323 K [22]. It should be noted that the picture of CO_2 molecules making discrete diffusive jumps by escaping their hydration cages is an interpretation based on the observed Arrhenius behavior, rather than on direct visualization of individual molecular trajectories. An alternative mechanism—in which CO_2 moves within a partially retained hydration shell without a distinct cage-escape event—cannot be ruled out by the present MSD- and RDF-based analyses. Future studies employing residence-time analysis of water molecules in the CO_2 hydration shell would help to distinguish these two microscopic pictures. Nevertheless, regardless of the detailed mechanism, the pronounced temperature sensitivity confirms the dominant role of thermal activation in CO_2 transport. In the temperature range investigated, temperature is the dominant factor controlling CO_2 transport in saline aquifers.

2.1.3. Influence of Pressure

Figure 2C shows how the CO_2 diffusion coefficient changes with pressure at 3.5 mol/L NaCl and 313 K. Between 3 and 30 MPa, D increases slightly from 3.60×10^{-9} to 3.87×10^{-9} m^2/s (approximately 7.5%). This is consistent with other studies reporting that pressure exerts only a minor influence on CO_2 diffusion under typical storage conditions [18]. The weak increase occurs because the solution density varies only slightly in this pressure range, so the free volume available for molecular displacement does not change significantly.

However, when the pressure increases to 40 MPa, D decreases markedly to 3.29×10^{-9} m^2/s—approximately 15% lower than at 30 MPa. This observation suggests that at pressures above ~30 MPa, the reduction in free volume may begin to outweigh any facilitating effects on molecular displacement, though additional data points between 30 and 40 MPa would be needed to confirm this trend. Above about 30 MPa, the solution density becomes sufficiently high to outweigh any facilitating effects on molecular movement. The denser solution reduces free volume and increases friction, and CO_2 diffusion is retarded. This indicates that in very deep formations (deeper than ~2.5–3 km, assuming a geobaric gradient of ~10 MPa/km), pressure may hinder CO_2 movement, suggesting that the conventional view—that pressure is a secondary factor for CO_2 diffusion—may require qualification for ultra-deep reservoirs. Overall, in the typical storage pressure range (10–30 MPa), pressure is not the primary controlling factor for CO_2 diffusion. However, the threshold identified at 40 MPa suggests that caution should be exercised when using diffusion data for ultra-deep saline aquifers.

To verify the reliability of the diffusion coefficients, the MSD curves for representative conditions are shown in Figure 3. The linear region employed for fitting (10–50 ns) yielded $R^2 > 0.99$, confirming that the Einstein relation is satisfied.

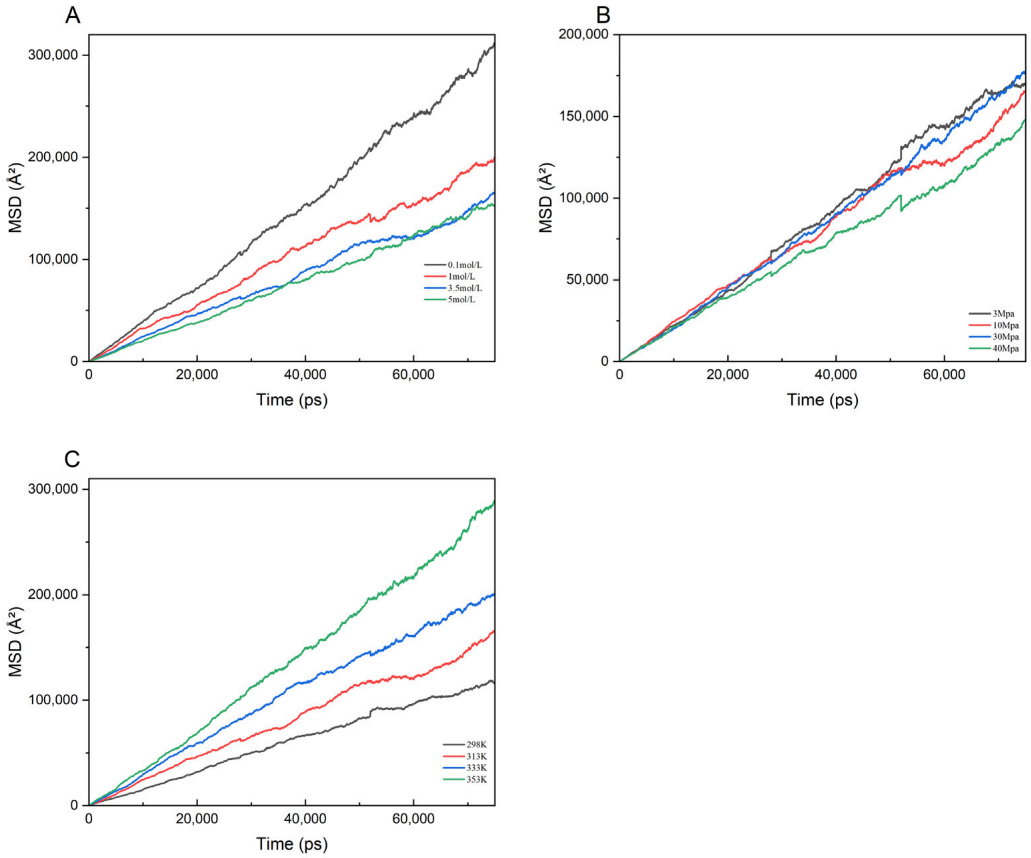


Figure 3. Mean square displacement (MSD) of CO_2 molecules in brine under different conditions. (**A**) Varying NaCl concentrations at 313 K and 10 MPa; (**B**) varying temperatures at 3.5 mol/L NaCl and 10 MPa; (**C**) varying pressures at 3.5 mol/L NaCl and 313 K.

2.2. Radial Distribution Function Analysis of CO_2 with Water and Ions

To investigate how salt concentration, temperature, and different ions affect the local hydration structure around CO_2, the radial distribution functions g(r) were calculated between CO_2 and water oxygen, Na^+, and Cl^-. By examining the first peak position, peak height, and coordination number, the local arrangement of water molecules around CO_2 and the influence of ions on this structure were characterized.

2.2.1. Influence of Salinity on the CO_2–Water RDF

Figure 4A shows that when NaCl concentration increases from 0.1 to 5.0 mol/L, the first peak of the CO_2–O(H_2O) RDF increases (from 1.45 to 1.55), but the peak position remains at approximately 3.8 Å. A higher peak indicates water molecules are packed more densely around CO_2, forming a more ordered local structure. From the coordination numbers in Table 1, the results indicate that the number of water molecules in the first hydration shell remains nearly constant at approximately 4.0. Thus, the shell becomes denser through compression, rather than through incorporation of additional water molecules. This occurs because ions compete for water: Na^+ and Cl^- form strong hydration shells that consume substantial free water, and the remaining water is confined more tightly around CO_2. A denser hydration shell hinders CO_2 mobility, which is consistent with the decrease in diffusion coefficient with salinity reported in Section 2.1.

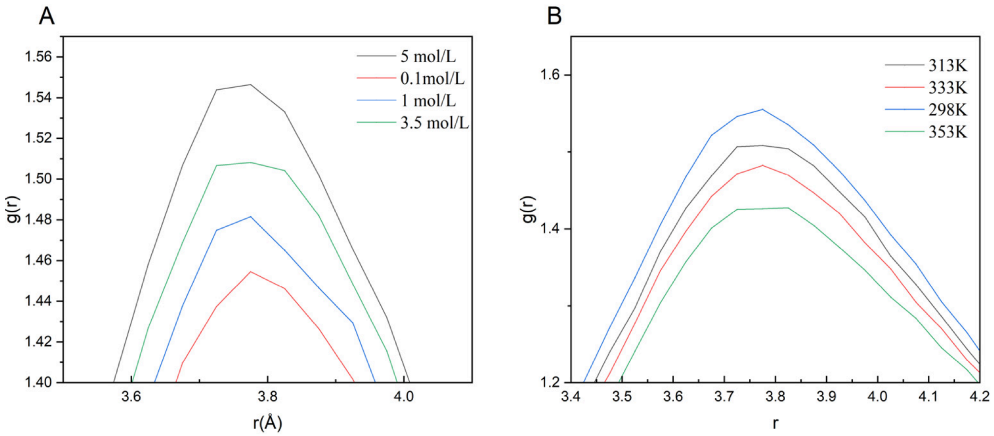


Figure 4. Radial distribution functions of CO_2 in brine. (**A**) CO_2–O(H_2O) RDF at different NaCl concentrations (313 K, 10 MPa); (**B**) CO_2–O(H_2O) RDF at different temperatures (3.5 mol/L NaCl, 10 MPa).

Table 1. Coordination number of the first hydration shell of CO_2 at different NaCl concentrations.

NaCl Conc. (mol/L)	First Peak Position	First Peak Height	Coordination Number
0.1	3.775	1.45452194	3.99472022
1	3.775	1.48152024	4.10263477
3.5	3.775	1.50814863	3.94462619
5	3.775	1.54645008	3.99684815

2.2.2. Influence of Temperature on the CO_2–Water RDF

Figure 4B shows that as temperature increases from 298 to 353 K, the first CO_2–O(H_2O) RDF peak decreases and broadens, and the peak position shifts slightly from about 3.7 to 3.8 Å. These changes indicate that stronger thermal motion disrupts the ordered water structure around CO_2, resulting in a more uniform local distribution. At 298 K, water molecules exhibit less thermal motion and can form a tighter hydration layer around CO_2, yielding a higher g(r) peak. This microstructural change explains why the diffusion coefficient increases significantly with temperature in Section 2.1: thermal energy weakens the hydration cage, thereby enhancing CO_2 mobility.

2.2.3. CO_2–Ion Radial Distribution Functions

Figure 5 compares the RDFs of CO_2–Na^+ and CO_2–Cl^- at 3.5 mol/L NaCl. CO_2–Na^+ shows a clear peak at about 3.3 Å (g(r) ≈ 1.18) and a shallow dip near 4.0 Å. CO_2–Cl^-, in contrast, exhibits no distinct peaks and remains near 1.0 over the entire range. This difference arises from the charge distribution in CO_2. Na^+ is attracted to the negatively charged oxygen atoms of CO_2, but Cl^- is repelled by those same negative charges, and Cl^- is further separated from CO_2 by its own strongly bound hydration shell. The CO_2–Na^+ peak is much lower than typical ion–water RDF peaks, indicating that this interaction is weak and transient. Therefore, direct blocking of CO_2 by ions is negligible, and the primary mechanism by which higher salinity retards diffusion remains the increase in solution viscosity and the densification of the CO_2 hydration shell.

To examine more closely the ordering of the first CO_2 hydration shell, the full width at half maximum (FWHM) of the first CO_2–O(H_2O) RDF peak was calculated. The results are presented in Figure 6. When NaCl concentration increases from 0.1 to 5.0 mol/L, the FWHM decreases slightly from approximately 1.19 to 1.17 Å, indicating that the hydration shell becomes marginally narrower. Together with the higher peak (Figure 4A) and the nearly

constant coordination number (Table 1), this confirms that the shell becomes denser rather than incorporating more water molecules. In contrast, when the temperature is raised from 298 to 353 K, the FWHM increases from about 1.10 to 1.24 Å, indicating pronounced thermal broadening. This is consistent with the lower peak in Figure 4B and directly reflects thermal disruption of the ordered hydration structure. The total FWHM change is within ~0.15 Å across all conditions, indicating that the first CO_2 hydration shell is structurally robust. The opposite FWHM responses to salinity and temperature provide a clear structural explanation for why the diffusion coefficient varies in opposite directions: a denser shell retards diffusion, while thermal broadening enhances it.

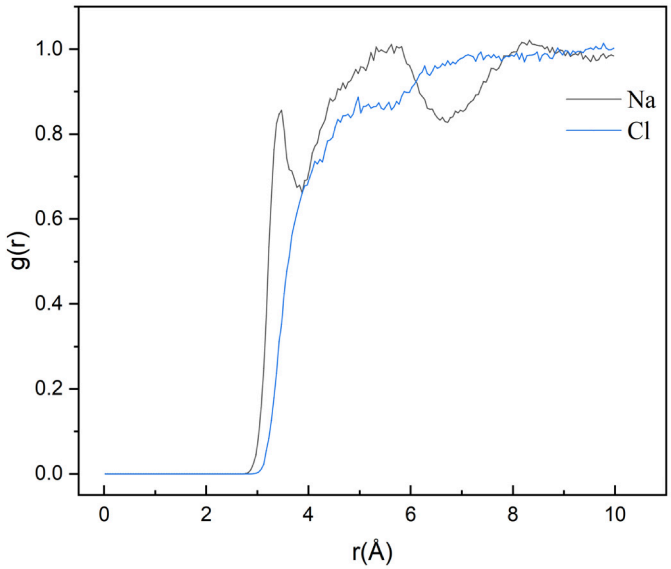


Figure 5. CO_2–Na^+ and CO_2–Cl^- RDF at 3.5 mol/L NaCl (313 K, 10 MPa).

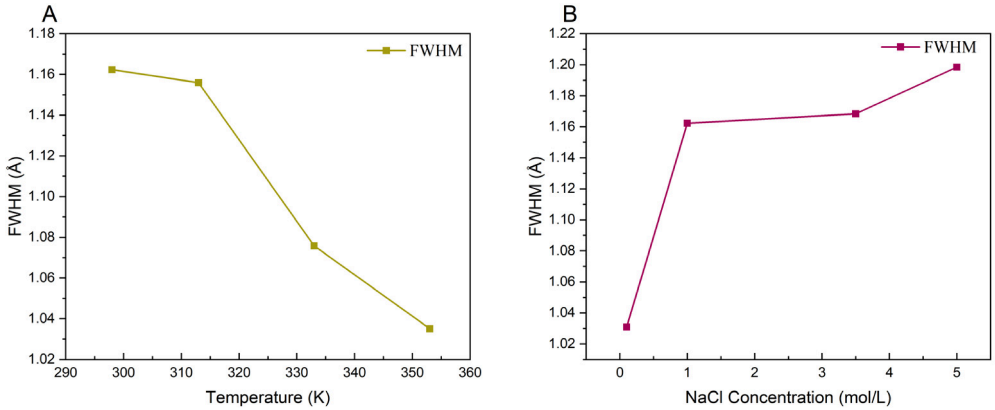


Figure 6. Full width at half maximum (FWHM) of the first CO_2–$O(H_2O)$ RDF peak as a function of (**A**) NaCl concentration and (**B**) temperature.

2.3. Changes in the Hydrogen Bond Network and the Role of Salt Ions

The extent to which salt ions perturb CO_2–water interactions was quantified through hydrogen bond analysis. The average number of hydrogen bonds per CO_2 molecule was calculated at different NaCl concentrations. A hydrogen bond was defined as O···H distance < 2.5 Å and O–H···O angle > 120°. The simulation system contained 53 CO_2 molecules, and Figure 7 shows the average hydrogen bond count per CO_2. When the NaCl concentration was increased from 0.1 to 5.0 mol/L, the average count decreased slightly, from 1.163 to 1.105—a decrease of approximately 5%. (At 0.1 and 1.0 mol/L, the values

overlapped within error.) This trend is consistent with the coordination numbers in Table 1 and shows that salt ions exert minimal influence on the local hydration around CO_2.

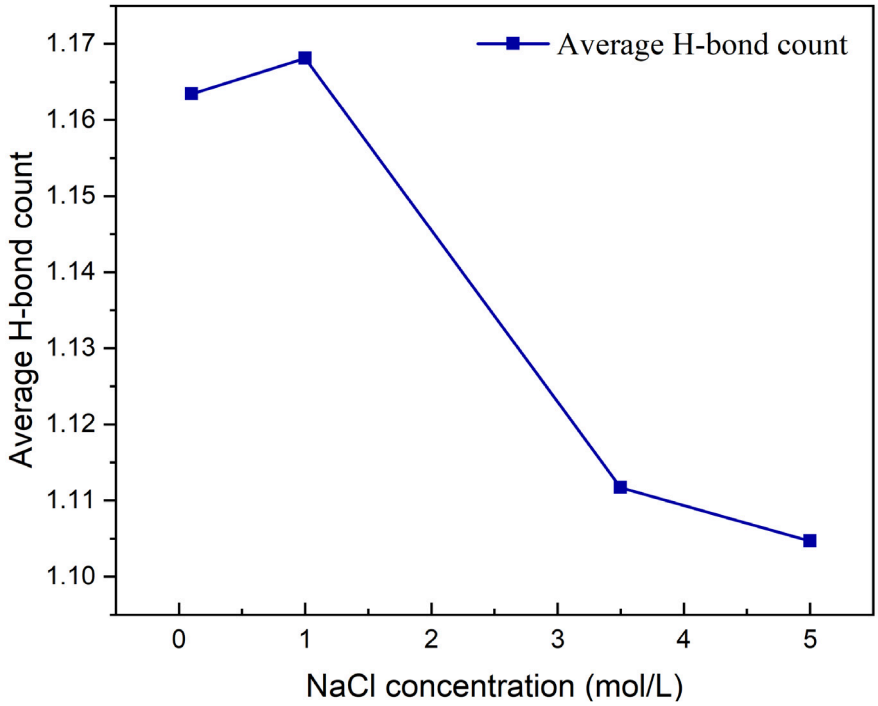


Figure 7. Average number of hydrogen bonds per CO_2 molecule with water at different NaCl concentrations.

A reduction in hydrogen bonds might superficially imply weaker attraction between CO_2 and water, which would allow CO_2 to diffuse faster. However, the diffusion coefficient decreases by approximately 50% as salinity increases. This marked contrast provides strong evidence that slower diffusion at high salinity is not caused by hydrogen bond disruption. Instead, it is primarily attributable to a significant increase in solution viscosity and steric hindrance from hydrated ions. At high salinity, ionic hydration shells start to overlap. This reduces the proportion of free water and increases the bulk viscosity, and increases the resistance to CO_2 motion.

While the CO_2–water hydrogen bond count remains nearly constant across the full salinity range, the water–water hydrogen bond network undergoes pronounced disruption. Figure 8 shows the average number of water–water hydrogen bonds per water molecule as a function of NaCl concentration. As the salinity increases from 0.1 to 5.0 mol/L, this number decreases substantially from 1.70 to 1.27, a reduction of approximately 25%. This decline reflects the progressive withdrawal of water molecules from the bulk hydrogen bond network into the hydration shells of Na^+ and Cl^-, consistent with the formation of contact ion pairs that sequester free water and elevate the solution viscosity.

Figure 9 illustrates this contrast clearly: when NaCl increases from 0.1 to 5.0 mol/L, hydrogen bonds per CO_2 decrease by only ~5%, but the diffusion coefficient decreases by ~50%. This mismatch, together with the concurrent disruption of the water–water hydrogen bond network (Figure 8), provides convergent evidence that salt ions retard CO_2 diffusion primarily through elevated solution viscosity and steric hindrance from hydrated ions, rather than through disruption of CO_2–water hydrogen bonds. It should be noted that the ~5% decrease in CO_2–water hydrogen bonds is based on a geometric definition (O···H < 2.5 Å, O–H···O > 120°), and fluctuations in hydrogen bond populations are inherent to MD simulations. The absolute hydrogen bond counts should therefore be interpreted with this sensitivity in mind; nevertheless, the qualitative conclusion—that

the change in hydrogen bonding is far smaller than the change in diffusion—is robust regardless of the specific cutoff values.

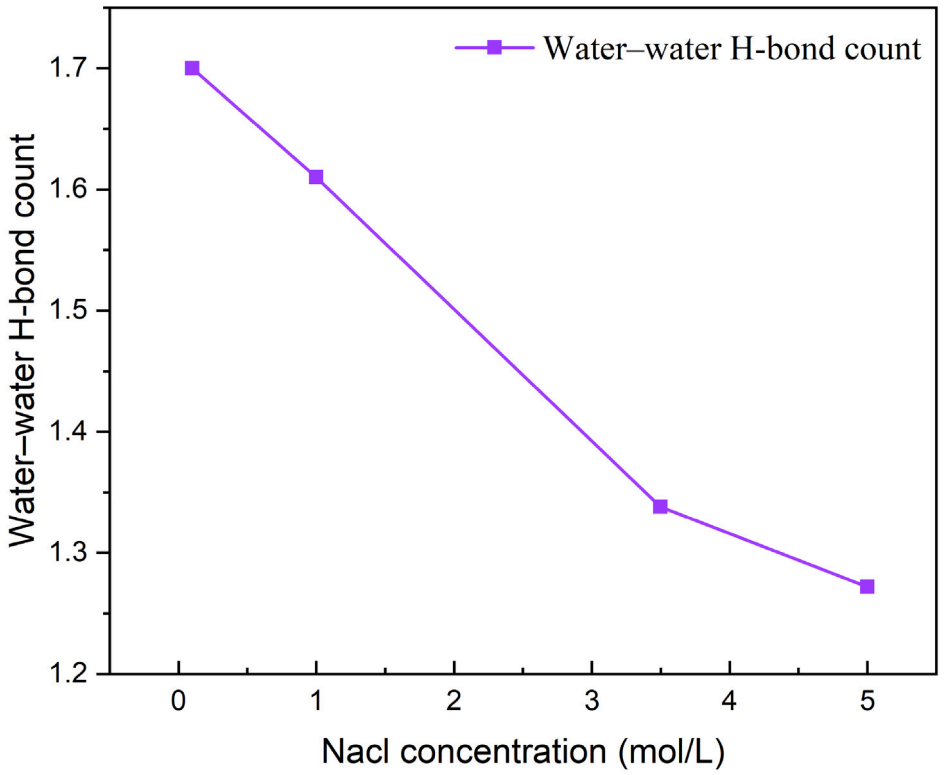


Figure 8. Average number of water–water hydrogen bonds per water molecule as a function of NaCl concentration at 313 K and 10 MPa.

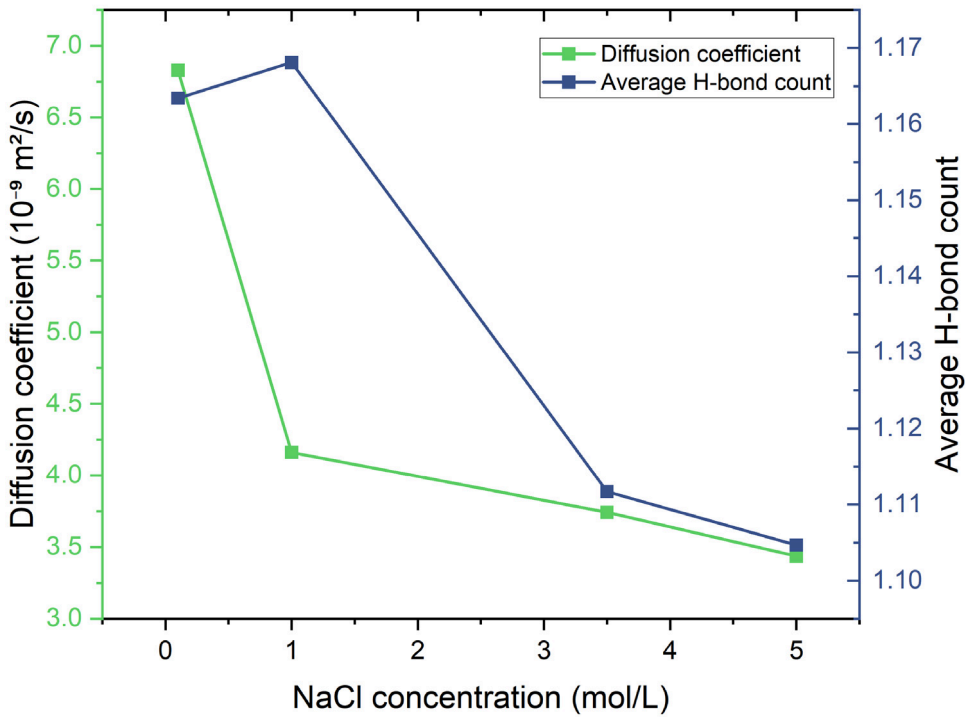


Figure 9. Comparison of the average number of hydrogen bonds per CO_2 molecule (left axis) and the CO_2 diffusion coefficient (right axis) as a function of NaCl concentration at 313 K and 10 MPa.

2.4. Comparison with Literature Results and Validation of Model Reliability

The simulation methodology was validated by comparing the CO_2 diffusion coefficients with published experimental and MD data. Polat et al. [23] reported a comprehensive review of both experiments and simulations for CO_2 diffusion in water.

Across the salinity range, the ~50% decline in D from 0.1 to 5.0 mol/L NaCl at 313 K and 10 MPa aligns with previous reports. Omrani et al. [18] found D reductions of 15–64% over 1–6 mol/kg NaCl from MD simulations; Cadogan et al. [24] confirmed the same trend using ^{13}C NMR at 298 K; and Perera et al. [22] measured a ~45% decrease in 4 mol/L NaCl by Raman spectroscopy. The quantitative differences among studies are modest and expected, given variations in force field parameterization, concentration units, and experimental conditions. What is consistent across all studies is the underlying mechanism: ions sequester free water into hydration shells (reflected in the 25% loss of water–water hydrogen bonds in Section 2.3), which raises bulk viscosity, while the CO_2 hydration shell simultaneously densifies without adding water molecules (higher g(r) peak, narrower FWHM, constant coordination number ≈ 4.0).

The temperature dependence also agrees well with the literature. The present activation energy of 13.8 kJ/mol falls within the 13.5–16.2 kJ/mol range reported by Omrani et al. [18]. This consistency across force fields suggests that the energy barrier for CO_2 diffusive jumps is fundamentally set by the reorganization of the surrounding hydrogen bond network. The RDF and FWHM analyses (Section 2.2.2) support this interpretation: elevated temperature broadens and lowers the first CO_2–$O(H_2O)$ peak, corresponding to thermal disruption of the ordered hydration cage that otherwise constrains CO_2 mobility.

Pressure effects are minor across 3–30 MPa (D varies by less than 10%), consistent with reports from Sell et al. [25], Perera et al. [22], and Omrani et al. [18]. The 15% drop observed at 40 MPa, however, suggests a threshold beyond which increased solution density and friction outweigh any facilitating contributions from local density fluctuations. This non-monotonic behavior warrants caution when extrapolating diffusion data to ultra-deep reservoirs (depth > ~3 km), where pressure-induced suppression may partially offset the thermal enhancement of CO_2 mobility.

It is worth noting an apparent tension with Chen et al. [17], who reported that dissolved CO_2 disrupts the hydrogen bond network and destabilizes ionic hydration shells in NaCl solutions. At first glance, this seems opposite to the present finding that CO_2–water hydrogen bonds are minimally affected by salinity. The two observations are, however, complementary rather than contradictory. Chen et al. examined how CO_2 perturbs pre-existing ion–water structures, whereas the present study examines how ions perturb CO_2–water interactions. The pronounced 25% reduction in water–water hydrogen bonds observed here (Figure 8) is in fact consistent with Chen et al.'s general picture of a disrupted water network—but the present work clarifies that ions, rather than CO_2, are the primary drivers of this disruption at high salinity. The CO_2–water hydrogen bond network, being far weaker than ion–water electrostatic interactions, is largely shielded from direct ionic perturbation; instead, it is the bulk reorganization of water into ionic hydration shells that raises the effective viscous resistance to CO_2 diffusion.

Taken together, the agreement with experimental and computational benchmarks confirms that the COMPASS force field adequately captures the key interactions governing CO_2 transport in brine. Minor discrepancies in absolute D values are attributable to force field version differences, system size effects on MSD statistics, and experimental uncertainties—none of which affect the mechanistic conclusions. Additionally, the simulation box dimensions (~33 Å per side) are relatively modest for diffusion calculations, and the Yeh–Hummer finite-size correction was not applied in this study. However, because

all systems share comparable box dimensions and the analysis focuses on relative trends across conditions rather than absolute D values, the comparative conclusions remain valid.

3. Materials and Methods

Molecular dynamics simulation is widely used to study atomic-scale transport. This method was selected for several reasons. First, the COMPASS force field has been specifically parameterized and tested for CO_2–water–alkali metal halide systems, and it yields reliable estimates for properties such as diffusion coefficients [26]. Second, homogeneous solution systems can be readily constructed with precise control over the amounts of CO_2, water, and ions, enabling accurate salinity control. Third, the simulation algorithms include thermostats and barostats that maintain temperature and pressure constant, making the method well-suited for studying transport under isothermal–isobaric conditions. The parameters of the constructed systems are shown in Table 2.

Table 2. Simulation System Parameter Table.

System	NaCl Conc. (mol/L)	H_2O Molecules	Na^+/Cl^- Pairs	CO_2 Molecules	Box Size (Å^3)
S0	0.1	1000	2	53	32.70 × 32.70 × 32.70
S1	1	1000	18	53	32.73 × 32.73 × 32.73
S2	3.5	1000	73	53	33.44 × 33.44 × 33.44
S3	5	1000	90	53	33.60 × 33.60 × 33.60

3.1. Model Structure

The brine system was constructed from water, CO_2, and NaCl. The initial three-dimensional structures of H_2O and CO_2 were obtained from the PubChem database [27,28], and standard ion models were adopted for Na^+ and Cl^-. Four systems were constructed with NaCl concentrations of 0.1, 1.0, 3.5, and 5.0 mol/L. Each system initially contained 1000 H_2O molecules and 53 CO_2 molecules, and the numbers of Na^+–Cl^- ion pairs were 2, 18, 73, and 90. These values were determined from the target salt concentrations and the CO_2 mole fraction. Initial box dimensions were estimated from the total number of molecules and the density of pure water at 313 K. After building the systems, energy minimization was performed to remove unfavorable atomic overlaps and relieve high-energy strain, with stringent convergence criteria (energy change $< 1 \times 10^{-5}$ kcal/mol; maximum force < 0.001 kcal/mol/Å). A short NVT equilibration was then performed, followed by an NPT equilibration at 313 K and 0.1 MPa to obtain realistic equilibrium densities. Table 1 lists the final system parameters after the NPT equilibration, and Figure 10 shows the constructed model.

3.2. Force Field and Parameters

The accuracy of molecular simulation depends on the force field. All simulations were performed using a commercial MD simulation platform. The COMPASS force field describes all interatomic interactions, with atomic charges assigned automatically. COMPASS has been specifically developed for modeling CO_2, water, and alkali metal halide solutions, and it has been widely tested for predicting transport properties such as density and diffusion coefficients in liquid mixtures [26]. It accurately captures CO_2–water, ion–water, and ion–CO_2 non-bonded interactions, enabling reliable simulation of CO_2 diffusion in brine.

Non-bonded interactions were treated as follows: electrostatic interactions were calculated with the Ewald summation method (accuracy 0.001 kcal/mol for NVT, 0.0001 kcal/mol for NPT, buffer width 0.5 Å). This study used the Lennard-Jones potential with an atom-based summation and cubic spline cutoff to model van der Waals

interactions. Cutoff distance was set to 15.5 Å, the spline width to 1 Å, and long-range corrections were applied.

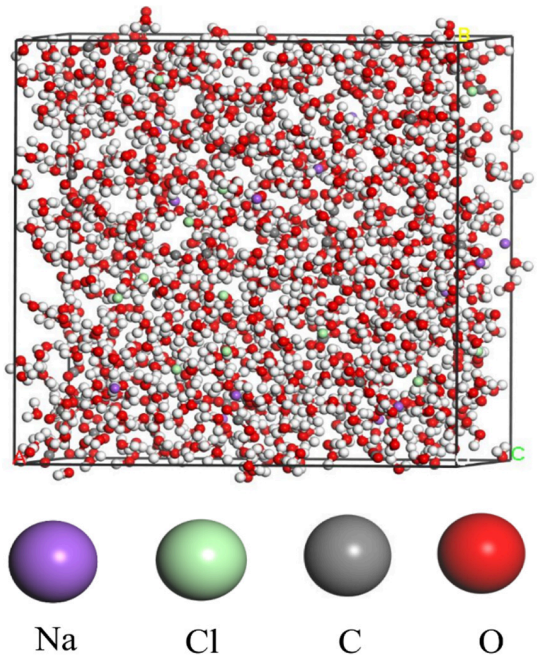


Figure 10. Schematic representation of the molecular dynamics model for CO_2 in NaCl brine (1.0 mol/L).

3.3. Simulation Details

The simulations were conducted in two stages: first, NPT equilibration; then, NVT production. During the NPT, the temperature was maintained at 313 K with a Nosé–Hoover thermostat (time constant = 0.1 ps) [29] and the pressure at 0.01 GPa (10 MPa) with a Berendsen barostat (pressure coupling time constant = 0.1 ps) [30]. A time step of 1.5 fs was used, and the equilibration was run for 1000 ps (approximately 666,667 steps).

After the NPT, NVT production runs of 100 ns were performed. Temperature was controlled using a Nosé–Hoover thermostat. The time step was 2.0 fs, yielding 50,000,000 steps. O–H bonds were constrained using the SHAKE algorithm, enabling a time step of 2.0 fs. To investigate the effects of salinity, temperature, and pressure on CO_2 diffusion, we designed a series of NVT runs using the controlled-variable method. The NaCl concentrations were set to 0.1, 1.0, 3.5, and 5.0 mol/L, the temperature ranged from 298 to 353 K, and the pressure from 3 to 40 MPa. Table 3 lists all the simulation conditions. All reported quantities were averaged over the final 50 ns of each NVT run, after confirming that the system had reached equilibrium.

Table 3. Summary of simulation cases for NVT production runs in this study.

Case	NaCl Conc. (mol/L)	Temperature (K)	Pressure (MPa)	Purpose
1	3.5	313	10	Baseline
2	0.1	313	10	Salinity effect
3	1	313	10	Salinity effect
4	5	313	10	Salinity effect
5	3.5	298	10	Temperature effect
6	3.5	333	10	Temperature effect
7	3.5	353	10	Temperature effect
8	3.5	313	3	Pressure effect
9	3.5	313	30	Pressure effect
10	3.5	313	40	Pressure effect

3.4. Diffusion Coefficient and Microscopic Analysis Methods

The tracer diffusion coefficient of CO_2 in brine was derived from the mean-square displacement (MSD) using the Einstein equation. MSD analysis was performed using standard modules within the MD platform. The linear region of the MSD curve was fitted, and the slope was substituted into the Einstein equation to obtain the diffusion coefficient D:

$$D = \frac{1}{6} \lim_{t \to \infty} \frac{d}{dt} \left\langle \mid r_i(t) - r_i(0) \mid^2 \right\rangle \quad (1)$$

where r_i(t) is the position of the i-th CO_2 molecule at time t, and the angle brackets mean the average over all CO_2 molecules and time origins. For some trajectories, the MSD showed non-physical drops at long times because of periodic boundary effects. In those cases, only the linear region before the first drop was used for fitting. The fitted region (10–50 ns) yielded an $R^2 > 0.99$. Statistical uncertainties in D were evaluated by block averaging: the final 50 ns of each NVT production run was divided into five 10 ns blocks, the MSD of each block was fitted independently, and the standard deviation of the five resulting D values is reported as the uncertainty in Table S1. The block-averaged uncertainties range from ±6% to ±35%, reflecting the intrinsic statistical fluctuation of CO_2 diffusion in these moderately sized simulation systems.

To investigate the effect of salt ions on the arrangement of water and ions around CO_2, the radial distribution functions g(r) were calculated between CO_2 and H_2O (oxygen), Na^+, and Cl^-. The carbon atom of CO_2 was used as the reference. The RDF calculations were based on the final 50 ns of each NVT run and used standard RDF analysis routines. The cutoff radius was set to 10.0 Å with a sampling interval of 0.05 Å, and only intermolecular pairs were considered. The position and height of the first peak in the RDF were used to determine the radius of the first CO_2 hydration shell and the coordination number, as well as to track how the hydration shell changes with salt concentration.

Hydrogen bond analysis was employed to examine how salt ions affect CO_2–water interactions. If this mechanism dominates, the average number of hydrogen bonds per CO_2 molecule should decrease substantially with increasing salinity. To evaluate this hypothesis, hydrogen bonds were quantified using a geometric criterion. A hydrogen bond was defined geometrically: an O···H distance of less than 2.5 Å and an O–H···O angle greater than 120°. A custom script was developed to analyze the NVT trajectories frame by frame and calculate the average number of hydrogen bonds per CO_2 molecule. This analysis enabled an assessment of how salt ions disrupt the CO_2–water hydrogen bond network.

4. Conclusions

In this work, MD simulations were employed to investigate the influence of NaCl concentration on CO_2 diffusion in saline aquifers, together with the effects of temperature and pressure. Diffusion coefficients were derived from MSD, and RDF and hydrogen bond analysis were used to elucidate the microscopic mechanisms. The main conclusions are as follows:

1. The CO_2 diffusion coefficient in brine decreases steadily as NaCl concentration increases. At 313 K and 10 MPa, when NaCl increases from 0.1 to 5.0 mol/L, D decreases by approximately 50% (from 6.83×10^{-9} to 3.44×10^{-9} m^2/s). This salting-out effect arises from the hydration of Na^+ and Cl^-, which increases solution viscosity and densifies the CO_2 hydration shell.
2. Temperature strongly enhances CO_2 diffusion. At 3.5 mol/L NaCl and 10 MPa, D increases by approximately 149% from 298 to 353 K (2.69×10^{-9} to 6.70×10^{-9} m^2/s), following Arrhenius behavior. Higher temperature increases molecular motion and weakens ion hydration, facilitating CO_2 migration.

3. Pressure exerts a minor influence on CO_2 diffusion between 3 and 30 MPa (variation < 8%). However, at 40 MPa, D decreases by approximately 15%, indicating that under very high pressure, the denser solution and reduced free volume begin to suppress diffusion. Under typical storage conditions (10–30 MPa), pressure is not the primary controlling factor, but caution is required for very deep reservoirs.
4. RDF analysis shows that with increasing NaCl concentration, the first CO_2–O(H_2O) peak height increases while the coordination number remains around 4.0, indicating that the hydration shell becomes denser rather than larger. CO_2–Na^+ exhibits a weak peak near 3.3 Å, whereas CO_2–Cl^- shows no distinct structure; therefore, direct ion blocking is negligible.
5. Hydrogen bond analysis shows that the average number of hydrogen bonds per CO_2 decreases only slightly (from 1.16 to 1.10) when salinity increases, while the water–water hydrogen bond count per molecule decreases substantially from 1.70 to 1.27. This contrast demonstrates that salt ions retard CO_2 diffusion primarily through increased viscosity and steric hindrance from hydrated ions, rather than by disrupting CO_2–water hydrogen bonds.

Supplementary Materials: The following supporting information can be downloaded at: https://www.mdpi.com/article/10.3390/molecules31122043/s1, Figure S1: Mean square displacement (MSD) curves of CO_2 at different NaCl concentrations (313 K, 10 MPa); Figure S2: Representative MSD curve with linear fitting for CO_2 at 3.5 mol/L NaCl, 313 K and 10 MPa ($R^2 > 0.99$); Figure S3: MSD curves of CO_2 at different pressures (3.5 mol/L NaCl, 313 K); Figure S4: MSD curves of CO_2 at different temperatures (3.5 mol/L NaCl, 10 MPa); Figure S5: Radial distribution functions g(r) for CO_2–O(H_2O) at different temperatures (3.5 mol/L NaCl, 10 MPa); Figure S6: Radial distribution functions g(r) for CO_2–O(H_2O) at different NaCl concentrations (313 K, 10 MPa); Table S1: Detailed diffusion coefficients of CO_2 under all simulated conditions with standard deviations (salinity, temperature, pressure) with standard deviations.

Author Contributions: Conceptualization, D.L.; Methodology, T.Z.; Software, T.Z.; Validation, T.Z., D.L.; Formal analysis, T.Z.; Investigation, T.Z.; Resources, D.L.; Data curation, T.Z.; Writing—original draft preparation, T.Z.; Writing—review and editing, D.L.; Visualization, T.Z.; Supervision, D.L.; Project administration, D.L.; Funding acquisition, D.L. All authors have read and agreed to the published version of the manuscript.

Funding: This research and the APC were funded by the National Natural Science Foundation of China (Grant 52304032) and the Future Plan Program for Young Scholars of Shandong University.

Data Availability Statement: The original contributions presented in this study are included in the article/Supplementary Materials. Further inquiries can be directed to the corresponding author.

Conflicts of Interest: The authors declare no conflicts of interest.

References

1. Hanson, E.; Nwakile, C.; Hammed, V.O. Carbon capture, utilization, and storage (CCUS) technologies: Evaluating the effectiveness of advanced CCUS solutions for reducing CO_2 emissions. *Results Surf. Interfaces* **2025**, *18*, 100381. [CrossRef]
2. Nagireddi, S.; Agarwal, J.R.; Vedapuri, D. Carbon Dioxide Capture, Utilization, and Sequestration: Current Status, Challenges, and Future Prospects for Global Decarbonization. *ACS Eng. Au* **2023**, *4*, 22–48. [CrossRef]
3. Global CCS Institute. *Global Status of CCS 2024: Scaling Up to Meet the Challenge*; Global CCS Institute: Melbourne, Australia, 2024. Available online: https://www.globalccsinstitute.com/resources/global-status-report/ (accessed on 13 March 2026).
4. IEA. *CCUS Projects Around the World Are Reaching New Milestones*; International Energy Agency Commentary: Paris, France, 2025. Available online: https://www.iea.org/commentaries/ccus-projects-around-the-world-are-reaching-new-milestones (accessed on 13 March 2026).

5. Bentham, M.; Kirby, G. CO_2 storage in saline aquifers. *Oil Gas Sci. Technol.* **2005**, *60*, 559–567. [CrossRef]
6. IPCC. *IPCC Special Report on Carbon Dioxide Capture and Storage*; Metz, B., Davidson, O., de Coninck, H.C., Loos, M., Meyer, L.A., Eds.; Cambridge University Press: Cambridge, UK, 2005. Available online: https://www.ipcc.ch/report/carbon-dioxide-capture-and-storage/ (accessed on 16 March 2026).
7. Wang, Q.G.; Zhang, D.X.; Li, Y.Q.; Li, C.Y.; Tang, H.Y. Numerical simulation study of CO_2 storage capacity in Deep Saline aquifers. *Sci. Technol. Energy Transit.* **2024**, *79*, 12. [CrossRef]
8. Dong, C.G.; Jiang, J.J.; Ye, B.; Xia, C.Y.; Zhang, Y.A. LCA-based cost-benefit assessment and carbon footprint accounting of CCUS technologies in China. *J. Clean. Prod.* **2025**, *486*, 144557. [CrossRef]
9. Izadpanahi, A.; Blunt, M.J.; Kumar, N.; Ali, M.; Tassinari, C.C.G.; Sampaio, M.A. A review of carbon storage in saline aquifers: Mechanisms, prerequisites, and key considerations. *Fuel* **2024**, *369*, 131744. [CrossRef]
10. Andreev, M.; de Pablo, J.J.; Chremos, A.; Douglas, J.F. Influence of Ion Solvation on the Properties of Electrolyte Solutions. *J. Phys. Chem. B* **2018**, *122*, 4029–4034. [CrossRef] [PubMed]
11. Fagorite, V.I.; Onyekuru, S.O.; Opara, A.; Oguzie, E.E. The major techniques, advantages, and pitfalls of various methods used in geological carbon sequestration. *Int. J. Environ. Sci. Technol.* **2023**, *20*, 4585–4614. [CrossRef]
12. Zhang, L.H.; Zhang, T.; Zhao, Y.L.; Hu, H.; Wen, S.; Wu, J.; Cao, C.; Wang, Y.; Fan, Y. A Review of Interaction Mechanisms and Microscopic Simulation Methods for CO_2-Water-Rock System. *Pet. Explor. Dev.* **2024**, *51*, 223–238. [CrossRef]
13. Coelho, F.M.; Franco, L.F.M.; Firoozabadi, A. Effect of Salinity on CO_2 Thermodiffusion in Aqueous Mixtures by Molecular Dynamics Simulations. *ACS Sustain. Chem. Eng.* **2023**, *11*, 17086–17097. [CrossRef]
14. Liu, A.X.; Liu, P.; Sun, Q.; Liao, Z.X. The experimental and modeling studies on the diffusion coefficient of CO_2 in pure water. *J. Petrochem. Univ.* **2012**, *25*, 5–9.
15. Zhang, H.; Al Kobaisi, M.; Zhang, Y.; Arif, M. CO_2 geological storage in subsurface aquifers as a function of brine salinity: A field-scale numerical investigation. *Geoenergy Sci. Eng.* **2025**, *245*, 213505. [CrossRef]
16. Carroll, J.J.; Slupsky, J.D.; Mather, A.E. The solubility of carbon dioxide in water at low pressure. *J. Phys. Chem. Ref. Data* **1991**, *20*, 1201–1209. [CrossRef]
17. Chen, C.; Zhang, K.; Wang, P.; Li, W.Z.; Song, Y.C.; Zhang, N. Ion Hydration and Hydrogen Bond Structure in NaCl Solutions at Temperatures and Pressures for Carbon Dioxide Sequestration: The Effects of Solvated CO_2 Molecules. *Mol. Phys.* **2014**, *112*, 74–84. [CrossRef]
18. Omrani, S.; Ghasemi, M.; Mahmoodpour, S.; Shafiei, A.; Rostami, B. Insights from molecular dynamics on CO_2 diffusion coefficient in saline water over a wide range of temperatures, pressures, and salinity: CO_2 geological storage implications. *J. Mol. Liq.* **2022**, *345*, 117868. [CrossRef]
19. Song, Y.; Chen, C.; Hu, W. *Understanding Geologic Carbon Sequestration and Gas Hydrate from Molecular Simulation*; Elsevier: Amsterdam, The Netherlands, 2024; ISBN 978-0-443-21888-0.
20. Li, Z.; Zhao, L.; Kou, J.; Wang, X. Electric Field-Enhanced CO_2 Dissolution and Adsorption for Geological Carbon Sequestration in Saline Aquifers. *Appl. Surf. Sci.* **2025**, *686*, 162147. [CrossRef]
21. Ding, W.; Jiang, T.T.; Chen, W.Y.; Hu, D.W.; Zhou, H.; Yang, F.J. Experimental study on CO_2-brine-sandstone interaction and reservoir stability analysis under high temperature and high pressure. *Renew. Energy* **2025**, *249*, 123146. [CrossRef]
22. Perera, P.N.; Deng, H.; Schuck, P.J.; Gilbert, B. Diffusivity of carbon dioxide in aqueous solutions under geologic carbon sequestration conditions. *J. Phys. Chem. B* **2018**, *122*, 4566–4572. [CrossRef] [PubMed]
23. Polat, H.M.; Coelho, F.M.; Vlugt, T.J.H.; Mercier Franco, L.; Tsimpanogiannis, I.N.; Moultos, O.A. Diffusivity of CO_2 in H_2O: A review of experimental studies and molecular simulations in the bulk and in confinement. *J. Chem. Eng. Data* **2024**, *69*, 3296–3329. [CrossRef]
24. Cadogan, S.P.; Hallett, J.P.; Maitland, G.C.; Trusler, J.P.M. Diffusion coefficients of carbon dioxide in brines measured using ^{13}C pulsed-field gradient nuclear magnetic resonance. *J. Chem. Eng. Data* **2015**, *60*, 181–184. [CrossRef]
25. Sell, A.; Fadaei, H.; Kim, M.; Sinton, D. Measurement of CO_2 diffusivity for carbon sequestration: A microfluidic approach for reservoir-specific analysis. *Environ. Sci. Technol.* **2013**, *47*, 71–78. [CrossRef]
26. Sun, H. COMPASS: An ab initio force-field optimized for condensed-phase applications—Overview with details on alkane and benzene compounds. *J. Phys. Chem. B* **1998**, *102*, 7338–7364. [CrossRef]
27. PubChem. Carbon Dioxide. Available online: https://pubchem.ncbi.nlm.nih.gov/compound/280 (accessed on 3 November 2025).
28. PubChem. Water. Available online: https://pubchem.ncbi.nlm.nih.gov/compound/962 (accessed on 3 November 2025).

29. Nose, S. A unified formulation of the constant temperature molecular dynamics methods. *J. Chem. Phys.* **1984**, *81*, 511–519. [CrossRef]
30. Berendsen, H.J.C.; Postma, J.P.M.; van Gunsteren, W.F.; DiNola, A.; Haak, J.R. Molecular dynamics with coupling to an external bath. *J. Chem. Phys.* **1984**, *81*, 3684–3690. [CrossRef]

Disclaimer/Publisher's Note: The statements, opinions and data contained in all publications are solely those of the individual author(s) and contributor(s) and not of MDPI and/or the editor(s). MDPI and/or the editor(s) disclaim responsibility for any injury to people or property resulting from any ideas, methods, instructions or products referred to in the content.